J. Fluid Mech. (1981), *vol.* 103, *pp.* 465–478
Printed in Great Britain

Penetration of free convection into a lateral cavity

By ADRIAN BEJAN AND SHIGEO KIMURA

Department of Mechanical Engineering,
University of Colorado,
Boulder, Colorado 80309

(Received 15 May 1980)

The paper presents a theoretical and experimental study of natural convection in a horizontal cavity which communicates laterally with a large reservoir. The cavity walls and the reservoir are at different temperatures. It is shown theoretically that the flow consists of a horizontal counterflow which penetrates the cavity over a distinct length. The penetration length is shown to be proportional to the cavity height and to the square root of the Rayleigh number based on cavity height and cavity–reservoir temperature difference. The validity of the theory is demonstrated on the basis of a flow visualization experiment. It is shown also that the Nusselt number for cavity–reservoir heat exchange is proportional to the square root of the Rayleigh number, and is relatively insensitive to the Prandtl number in the Pr range 0·7 to ∞. The energy-engineering applications of the lateral penetration flow are discussed.

1. Introduction

The objective of this paper is to report a fundamental study of the phenomenon of free convection penetration into a lateral (horizontal) cavity. The penetrative flow is driven by the temperature difference between the walls of the cavity and the fluid reservoir with which the cavity communicates. This flow has not been studied previously, yet it has important practical applications in the field of energy engineering. Specifically, the phenomenon of lateral penetration is responsible for the enhancement of heat transfer between fluids and irregular vertical walls with cavities. The enhancement of fluid motion and thermal mixing is an important consideration in the design of nuclear reactor core structures and superconducting magnets, as well as in the design of energy-efficient walls for buildings. The lateral penetration flow is also important in the heat transfer performance of strip finned vertical surfaces with the fins oriented horizontally.

The fluid mechanics literature contains considerable information on a phenomenon related to lateral penetration by free convection, namely, the interaction of a fluid reservoir with a vertical cavity into a horizontal wall (the open thermosyphon problem). This body of research was motivated by the need to invent adequate cooling arrangements of highly-stressed rotor blades of high-temperature gas turbines. The theoretical work on the open thermosyphon problem was pioneered by Lighthill (1953) who predicted, among a number of features, the laminar penetration length of cold reservoir fluid into a heated vertical tube with the bottom end closed. Lighthill's predictions were later confirmed by experimental measurements reported by Martin & Cohen (1954), Martin (1955) and Hasegawa, Nishikawa & Yamagata (1963). In a related

0022–1120/81/4664–3410 $01.50

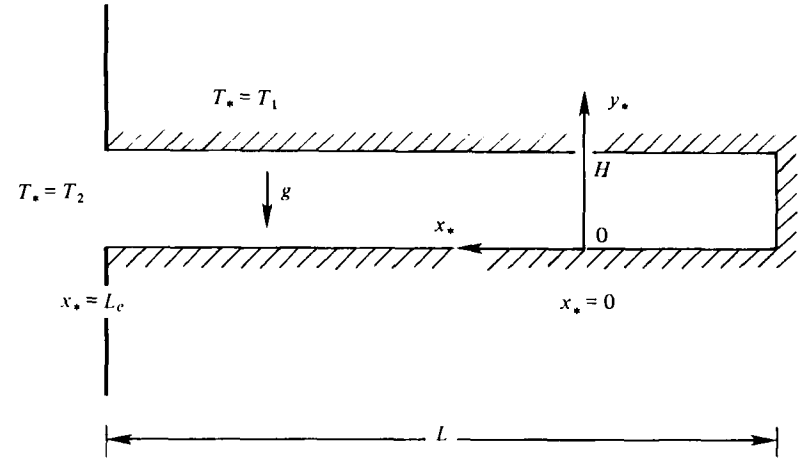

FIGURE 1. Schematic diagram of two-dimensional cavity communicating laterally with a fluid reservoir.

study, Martin (1959) determined experimentally the effect of tube inclination (departure from the vertical orientation) on the boundary-layer flow induced in the tube. The maximum angular departure considered in this experiment was 51·5 °. A comprehensive review of these and other advances in the area of free convection penetration into vertical cavities was written by Bayley & Martin (1971). This review shows that the horizontal cavity problem remains to be documented.

In what follows, we describe the first study of free convection penetration into a horizontal two-dimensional cavity. The paper has three parts. In the next section we develop the proper scaling and analytical formulation of the penetrative flow. Next, we report numerical results obtained based on the preceeding theory. Finally, in § 4, we report experimental observations on the flow pattern which agree well with the theory. We conclude the paper with a discussion of the engineering importance of our results in the calculation of heat transfer rates from vertical walls with lateral cavities or with extended surfaces (fins).

2. Theory

Consider the two-dimensional lateral cavity of length L and height H shown in figure 1. The solid walls of the cavity are maintained at a temperature T_1, while the fluid reservoir communicating with the cavity is maintained at a temperature T_2.

If the cavity wall is warmer than the reservoir ($T_1 > T_2$), and if the fluid expands upon isobaric heating, the cavity fluid will become buoyant and rise into the adjacent reservoir. At the same time, cold fluid from the reservoir will creep into the cavity replacing the departing warm fluid. Hence, we expect a cavity flow which is, on the one hand, driven by the cavity–reservoir temperature difference and, on the other hand, retarded by wall friction. The friction effect will become more pronounced as the cavity slenderness increases ($H/L \to 0$). In fact, we can imagine a lateral cavity slender enough so that its extremity (closed end) is filled with isothermal fluid forever unaffected by the natural circulation induced by the reservoir. In such a cavity the

free convection exchange of fluid and heat is limited to a region near the mouth. One of the objectives of this investigation is to determine the distance to which reservoir fluid penetrates into the cavity.

Mathematical formulation

Let L_e be the unknown length of the 'entrance' zone of interest. Relative to the Cartesian system of co-ordinates x_*, y_* shown in figure 1, the equations governing the conservation of mass, momentum and energy can be written as

$$\frac{\partial u_*}{\partial x_*} + \frac{\partial y_*}{\partial v_*} = 0, \tag{1}$$

$$u_* \frac{\partial \zeta_*}{\partial x_*} + v_* \frac{\partial \zeta_*}{\partial y_*} = \nu \left(\frac{\partial^2 \zeta_*}{\partial x_*^2} + \frac{\partial^2 \zeta_*}{\partial y_*^2} \right) + \beta g \frac{\partial T_*}{\partial x_*}, \tag{2}$$

$$u_* \frac{\partial T_*}{\partial x_*} + v_* \frac{\partial T_*}{\partial y_*} = \alpha \left(\frac{\partial^2 T_*}{\partial x_*^2} + \frac{\partial^2 T_*}{\partial y_*^2} \right). \tag{3}$$

In these equations, u_*, v_*, T_*, ν, α, β are the x_* and y_* velocity components, temperature, kinematic viscosity, thermal diffusivity and coefficient of thermal expansion, respectively. The fluid medium is regarded as Boussinesq-incompressible, in other words, the density variations are neglected everywhere except in the buoyancy term in the momentum equation (2). Function $\zeta_*(x_*, y_*)$ appearing in the momentum equation is the vorticity function

$$\zeta_* = \frac{\partial^2 \psi_*}{\partial x_*^2} + \frac{\partial^2 \psi_*}{\partial y_*^2}, \tag{4}$$

while $\psi_*(x_*, y_*)$ is the stream function defined as

$$u_* = -\frac{\partial \psi_*}{\partial y_*}, \quad v_* = \frac{\partial \psi_*}{\partial x_*}, \tag{5, 6}$$

The boundary conditions accounting for the horizontal walls of the cavity ($y_* = 0, H$) are

$$\psi_* = 0, \quad \frac{\partial \psi_*}{\partial y_*} = 0, \quad T_* = T_1. \tag{7, 8, 9}$$

Conditions at $x_* = 0$ and at the mouth of the cavity ($x_* = L_e$) will account for the manner in which the cavity flow interacts with the rest of the cavity ($x_* < 0$) and the reservoir fluid. Since the interactions at $x_* = 0, L_e$ depend on the flow and temperature pattern in the $0 < x^* < L_e$ region, we postpone their discussion until § 3 where a solution for the flow field is determined.

Scaling

In the region of interest, $0 < x^* < L_e$, the directional gradients $\partial/\partial x_*$, $\partial/\partial y_*$ are of order l^{-1}, H^{-1}, where l is the horizontal length scale of the flow pattern. In the same region, temperature changes scale as the wall–reservoir temperature difference which drives the flow, $\Delta T = T_1 - T_2$. Assuming that the cavity flow pattern is slender, $H \ll l$, the balance of convection and diffusion in the energy equation (3),

$$\frac{\psi_* \Delta T}{Hl} \sim \frac{\alpha \Delta T}{H^2},$$

suggests that the stream function ψ_* is of order $\alpha l/H$. The balance of viscous and buoyancy forces in the momentum equation (2),

$$\frac{\nu}{H^2}\left(\frac{\psi_*}{H^2}\right) \sim \frac{\beta g \Delta T}{l},$$

implies that ψ_* is also of order $\beta g \Delta T H^4/(\nu l)$. We conclude that

$$\frac{\alpha l}{H} = \frac{\beta g \Delta T H^4}{\nu l} \quad \text{or} \quad \frac{l}{H} = \left(\frac{\beta g H^3 \Delta T}{\alpha \nu}\right)^{\frac{1}{4}}.$$

This is an important result which shows that the flow slenderness ratio l/H scales up as the square root of the Rayleigh number based on H and ΔT,

$$Ra = \frac{\beta g H^3 \Delta T}{\alpha \nu}. \tag{10}$$

Therefore, the appropriate non-dimensional variables of the problem are

$$x = \frac{x_*}{H\,Ra^{\frac{1}{2}}}, \quad y = \frac{y_*}{H}, \tag{11), (12}$$

$$\psi = \frac{\psi_*}{\alpha\, Ra^{\frac{1}{2}}}, \quad \theta = \frac{T - T_1}{T_1 - T_2}. \tag{13), (14}$$

The corresponding non-dimensional conservation statements are

$$\frac{1}{Pr}\left(-\frac{\partial\psi}{\partial y}\frac{\partial^3\psi}{\partial x\,\partial y^2} + \frac{\partial\psi}{\partial x}\frac{\partial^3\psi}{\partial y^3}\right) = \frac{\partial^4\psi}{\partial y^4} + \frac{\partial\theta}{\partial x}, \quad -\frac{\partial\psi}{\partial y}\frac{\partial\theta}{\partial x} + \frac{\partial\psi}{\partial x}\frac{\partial\theta}{\partial y} = \frac{\partial^2\theta}{\partial y^2}, \tag{15), (16}$$

where $Pr = \nu/\alpha$ is the Prandtl number. Note that the $\partial^2/\partial x_*^2$ terms appearing in the original equations have been neglected, based on the slender pattern assumption ($l \gg H$). The corresponding boundary conditions along the horizontal walls are

$$\psi = \frac{\partial\psi}{\partial y} = \theta = 0 \quad \text{at} \quad y = 0, 1. \tag{17}$$

Similarity pattern

Visual inspection of equations (15), (16) and conditions (17) reveals that the problem admits a similarity solution in which the longitudinal velocity (hence ψ) is proportional to x, and the cavity fluid temperature is proportional to x^2. Such a dependence on longitudinal position is physically plausible in view of the fact that at the deep end ($x = 0$) the fluid is motionless and isothermal. Substituting

$$\psi = x\phi(y), \quad \theta = x^2\tau(y) \tag{18), (19}$$

into equations (15), (16) yields

$$\frac{1}{Pr}(-\phi'\phi'' + \phi\phi''') = \phi'''' + 2\tau, \quad -2\phi'\tau + \phi\tau' = \tau'', \tag{20), (21}$$

where the primes denote d/dy. The boundary conditions (17) become

$$\phi = \phi' = \tau = 0 \quad \text{at} \quad y = 0, 1. \tag{22}$$

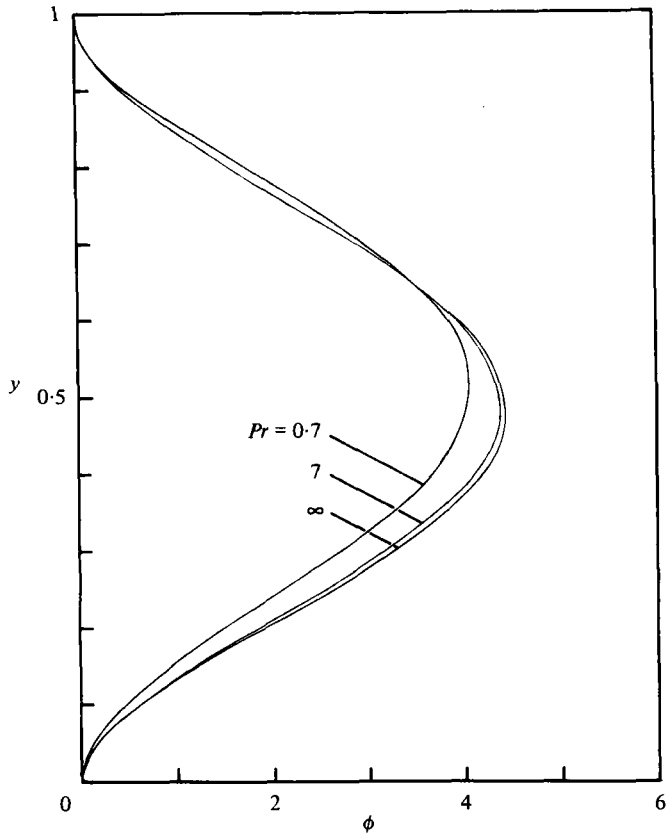

FIGURE 2. Stream-function profile as a function of Prandtl number.

It is interesting to note at this point that the longitudinal dependence of the flow and temperature fields, equations (18), (19), is not the same as in the vertical penetrative flow described by Lighthill (1953). In a vertical tube with one end open, the longitudinal velocity *and* the temperature vary linearly with longitudinal position; the same x-variation as in Lighthill's solution is exhibited by the similarity solution for natural convection in a vertical well filled with porous medium (Bejan 1980).

3. Numerical results

We solved equations (20), (21) numerically employing the shooting technique described in Carnahan, Luther & Wilks (1969). The numerical integration was based on the standard fourth-order Runge–Kutta method using 40 nodes equidistantly placed between $y = 0$ and $y = 1$. The integration was started from $y = 0$; the initial values of ϕ'', ϕ''' and τ' had to be adjusted successively until the $y = 1$ boundary conditions (22) were satisfied.

The success of each integration was assessed by calculating the three shooting errors in τ, ϕ and ϕ' at $y = 1$. We found the $\tau_{y=1}$ error to be most sensitive to the initial value selected for $\tau'_{y=0}$. The remaining two errors, $\phi_{y=1}$ and $\phi'_{y=1}$, were grouped into an aggregate function $E = (\phi_{y=1})^2 + (\phi'_{y=1})^2$ which is most sensitive to the values

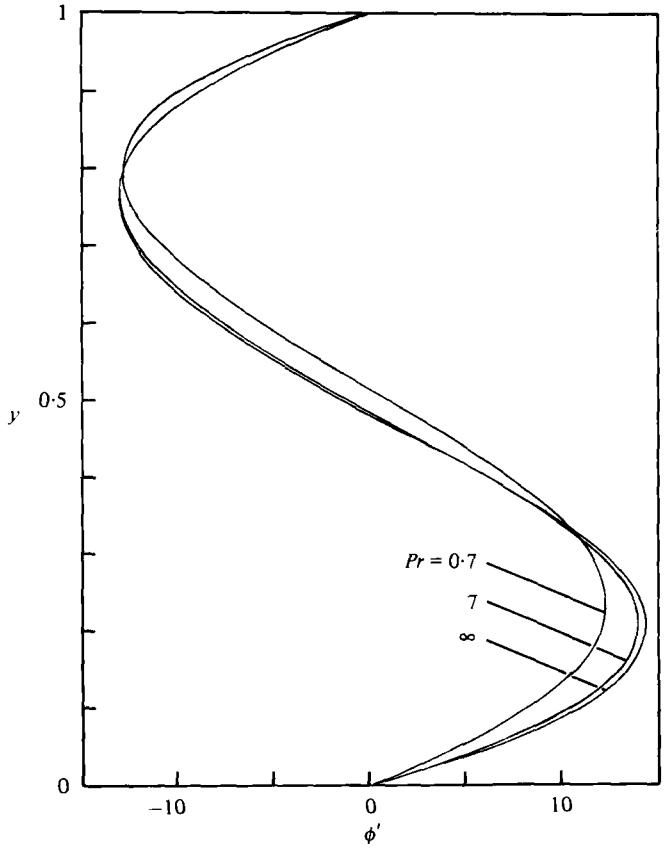

FIGURE 3. Horizontal velocity profile as a function of Prandtl number.

chosen for $\phi''_{y=0}$ and $\phi'''_{y=0}$. We minimized function E (i.e. we found the correct $\phi''_{y=0}$ and $\phi'''_{y=0}$), using the 'direct search method' proposed by Hooke & Jeeves (1961). We were also able to minimize the $\tau_{y=1}$ erorr by varying $\tau'_{y=0}$ and linearly interpolating between two consecutive erroneous guesses. The numerical solution presented below satisfies the following shooting success criterion

$$\left|\frac{\Phi_{y=1}}{\Phi_{\max}}\right| < 10^{-5},$$

where Φ represents functions τ, ϕ or ϕ', and $\Phi_{\max}$ is the absolute maximum attained by the respective function between $y = 0$ and $y = 1$.

Figures 2–4 show the numerical solution corresponding to three different Prandtl numbers, $Pr = 0{\cdot}7$ (air at 1 atm, 100 °C), $Pr = 7$ (pure water at 20·5 °C) and $Pr \to \infty$ (light oil). Using this solution, in figure 5 we plotted a set of streamlines (ψ = constant) and isotherms (θ = constant) for the limiting case $Pr \to \infty$.

The flow pattern consists of a horizontal counterflow increasing in intensity toward the mouth of the cavity. The streamline pattern is similar to Phillips' (1966) salinity-driven intrusion flow along the surface of the Red Sea. In the present case, cold fluid is drawn from the reservoir into the lower half of the cavity; next, the fluid warms up,

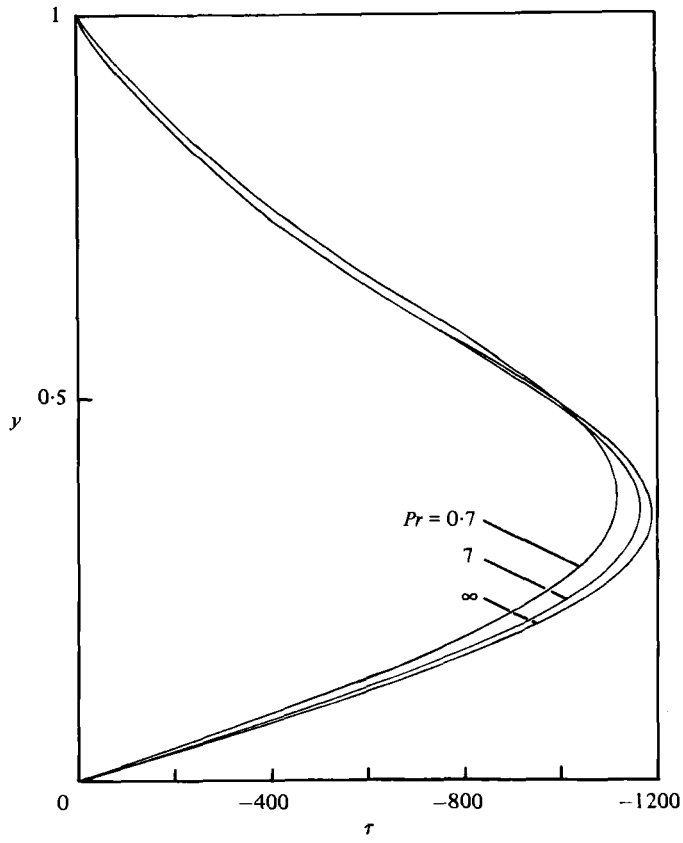

FIGURE 4. Temperature profile as a function of Prandtl number.

rises into the upper half of the cavity, turns aound and escapes back into the reservoir. The level where the horizontal velocity changes sign ($y = 0{\cdot}48$ for $Pr \to \infty$) migrates upward as the Prandtl number decreases (see y corresponding to $\phi' = 0$ in figure 3). The shift in the maximum of function $\phi(y)$ (figure 2) indicates that the total mass flow drawn into the cavity decreases as the Prandtl number decreases.

The temperature profile $\tau(y)$ (figure 4) demonstrates that, in an average sense, the fluid in the lower half of the cavity is colder than in the upper half. The temperature minimum is located at $y = 0{\cdot}349$ ($Pr \to \infty$); this minimum migrates upward as Pr decreases. The heating of the cavity fluid is most intense along the lower wall, where the inflow of cold fluid first comes in contact with the warm wall. The heating process is completed at a slower rate as the stream changes direction and sweeps the upper wall. The two wall temperature gradients and other features of the flow have been assembled in table 1.

The pattern displayed in figures 2–5 is the result of solving equations of the boundary layer type, where the $\partial^2/\partial x^2$ diffusion terms have been neglected. This solution cannot be expected to satisfy boundary conditions imposed on the vertical end-planes $x = 0$, $x = L_e/l$, because in the end regions the slender-pattern approximation does not apply. However, we can still account for end conditions by specifying the maximum temperature difference working across the similarity pattern. This approach is known to

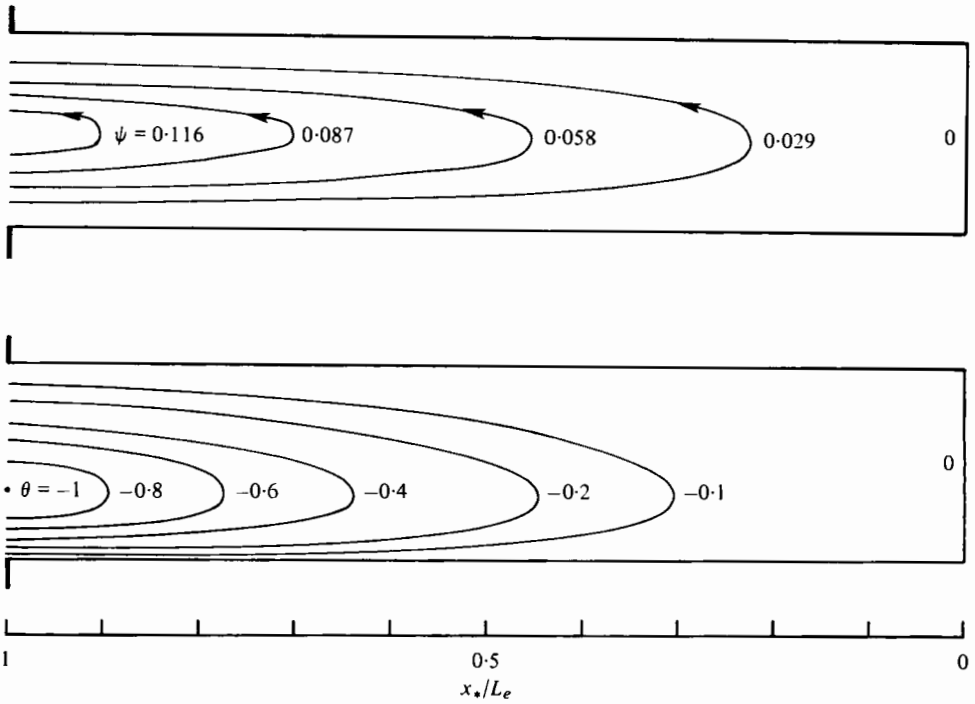

FIGURE 5. Streamlines and isotherms for the case $Pr \to \infty$.

Pr	$\tau'(y=0)$	$\tau'(y=1)$	$\tau_{\min}$	$y(\tau_{\min})$	L_e/l	$C = Nu/Ra^{\frac{1}{2}}$
0·7	−4483	1386	−1119·5	0·3711	0·02989	0·0522
0	−4984	1312	−1162·9	0·3514	0·02932	0·0529
∞	−5129	1321	−1185·8	0·3488	0·02904	0·0527

TABLE 1.

work satisfactorily, as demonstrated by Lighthill (1953) in the analysis of free convection penetration into a vertical tube, and by Bejan (1980) in the study of a vertical well filled with a fluid-saturated porous medium.

In the present solution, the temperature distribution satisfies already the condition $\theta = 0$ at the warm end ($x = 0$). At the opposite end, the entering fluid is all at T_2 (reservoir temperature), hence, we can *approximately* set the lowest temperature of the similarity pattern equal to the reservoir temperature ($\theta = -1$). This approximation is a fundamental feature of the present theory which, as discussed earlier, is based on solving equations of the parabolic type. Writing therefore

$$\theta_{\min} = (L_e/l)^2 \tau_{\min} = -1 \tag{23}$$

we find an important parameter of the flow field, namely, the horizontal dimension

$$\frac{L_e}{l} = \left(\frac{1}{-\tau_{\min}}\right)^{\frac{1}{2}} \tag{24}$$

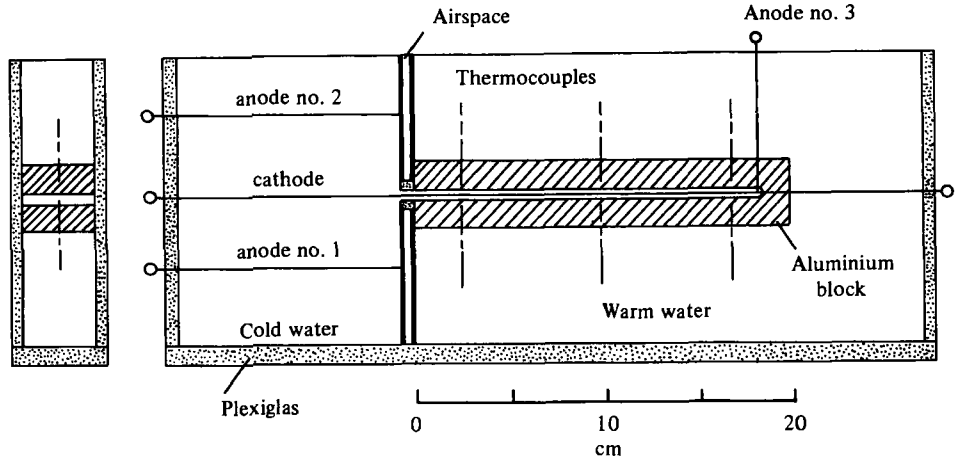

FIGURE 6. Scale drawing of the experimental apparatus.

or the slenderness ratio

$$\frac{L_e}{H} = \left(\frac{Ra}{-\tau_{\min}}\right)^{\frac{1}{3}} \tag{25}$$

As shown in table 1, for a wide range of Prandtl numbers the entrance length L_e is approximately 30 times less than the horizontal length scale l. From equation (25) we learn also that the Rayleigh number must be considerably greater than $1{\cdot}2 \times 10^3$ for the present theory to be valid, i.e. for $L_e/H \gg 1$.

Finally, keeping in mind that the similarity pattern exists as long as the cavity length L exceeds the flow length L_e, the Rayleigh number of the flow which just reaches the solid end of the cavity is

$$Ra_{\max} = (-\tau_{\min})(L/H)^2. \tag{26}$$

If Ra increases above this threshold value, we expect the similarity pattern (18), (19) to still be accurate everywhere except immediately near the end wall, provided $L_e/H = L/H \gg 1$. In the high Ra limit we envision reservoir fluid filling most of the cavity, except for a thin boundary layer lining the vertical end wall. It is possible also that in this limit the horizontal (warm) wall will be cooled down closer to the reservoir temperature, so that the fluid in the cavity becomes stably stratified. This effect will depend upon the heat transfer capability of the wall relative to the fluid (the inverse of the Biot modulus). Based on our own experimental observations (§ 4), we feel that the lower wall temperature will be affected by the flow, particularly in applications where the horizontal walls are not massive (e.g., the gap formed between two parallel horizontal strip fins on a vertical surface). This effect can also be present when $L_e < L$, i.e. for $Ra < Ra_{\max}$, as well as for $L_e = L$ with $Ra > Ra_{\max}$.

4. Experiment

We tested the preceding theory by conducting the small-scale experiment shown in figure 6. The central component of the experimental apparatus is a massive block of aluminium with a horizontal space milled into it (dimensions: height $H = 6{\cdot}4$ mm,

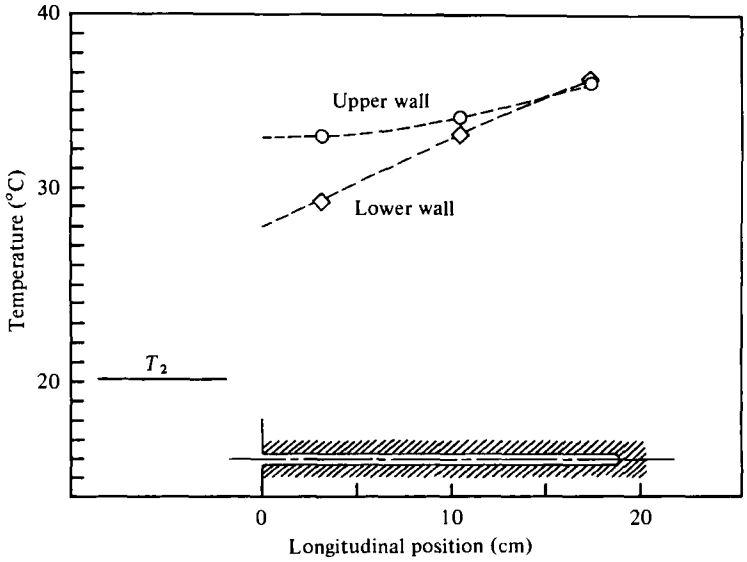

FIGURE 7. Measured temperature distribution along the horizontal walls of the cavity.

length $L = 181$ mm, width $W = 38{\cdot}4$ mm). The rest of the apparatus is a Plexiglas water basin with two separate compartments. In figure 6, the compartment on the left contains cold water and communicates with the horizontal space milled into the aluminium block. The compartment on the right-hand side is filled with warm water; its only function is to maintain the block heated to a temperature above that of the left compartment. The direct thermal contact between the two reservoirs was inhibited by constructing the vertical air layer (5 mm thick) shown in the scale drawing.

The objective of this experiment was to visualize and photograph the penetration length L_e of cold water into the warm lateral cavity. For flow visualization we used the pH indicator method described by Baker (1966): we filled the left compartment with water–thymol blue solution and applied 6V between the electrodes positioned as shown in figure 6. The cathode is the electrode which marks the solution deep blue; therefore, we mounted this electrode on the centre-line of the lateral cavity. The cathode and anode number 3 are electrically insulated from the aluminium block.

Figures 7 and 8 show one set of representative measurements. The photograph demonstrates that the cold (transparent) fluid protrudes into the lateral cavity to a distinct depth ($L_e \cong 7{\cdot}5$ cm). In the cavity, the cold fluid rises, sweeps past the cathode and darkens the upper half of the horizontal space. The upper half is darkest towards the tip of the flow ($x^* = 0$), because in this region the upflow is weak, i.e., unable to wash away the blue shed from the cathode. It is worth noting also that the swarm of small hydrogen bubbles collected on the cathode are responsible for striations which reproduce very well the streamline pattern of figure 5. In the stagnant zone ($x^* < 0$) the cavity appears dark above and below the cathode, because in this region the blue generated by the horizontal wire diffuses radially into stagnant fluid. In the cold reservoir (to the left of the lateral cavity) the buoyant flow is driven primarily by heat transfer across the air-insulated double wall. The reservoir flow consists of a

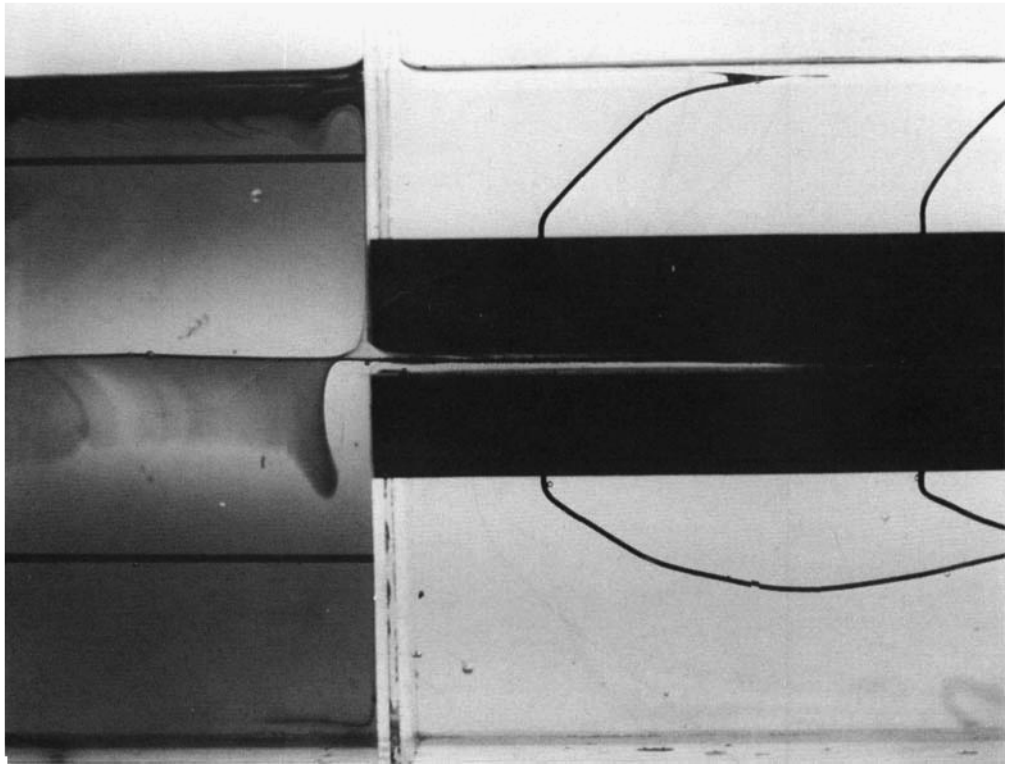

FIGURE 8. Penetration of free convection into a lateral cavity filled with water ($Pr \simeq 7$, $H = 6{\cdot}4$ mm, $L = 181$ mm). The corresponding temperature measurements are reported in figure 7.

boundary layer upflow along the air partition, plus a uniform downflow sufficiently far from the partition. The lateral cavity draws fluid from the vertical boundary layer.

The cavity wall temperature was recorded through six thermocouples imbedded in the aluminium block, close to the cavity wall. The location of these thermocouples is shown in figure 6. Measurements of the type reported in figure 7 demonstrate that the vertical air layer performs satisfactorily in insulating the warm metal channel from the cold reservoir. However, the cold fluid protruding into the lateral cavity has a visible cooling effect on the lower wall. Despite this effect, the walls of the latera cavity are roughly 15 °C warmer than the cold reservoir.

To test the quantitative results predicted by our analysis, we calculated the predicted penetration length L_e for the experiment shown in figures 7 and 8. Evaluating water properties at 30 °C and taking $\Delta T \cong 15$ °C, we found $Ra = 9{\cdot}6 \times 10^4$. Using equation (25) and table 1, the predicted length is $L_e = 9{\cdot}1\,H = 5{\cdot}8$ cm. This length agrees well with the photographed length, 7·5 cm. The difference (23 %) can be attributed only in part to the small buffer region effecting the transition from the reservoir to the similarity pattern representing the leading segment of the intrusion flow. As shown below, this difference is due primarily to an interesting effect induced by the temperature variation along the horizontal walls of the cavity (figure 7).

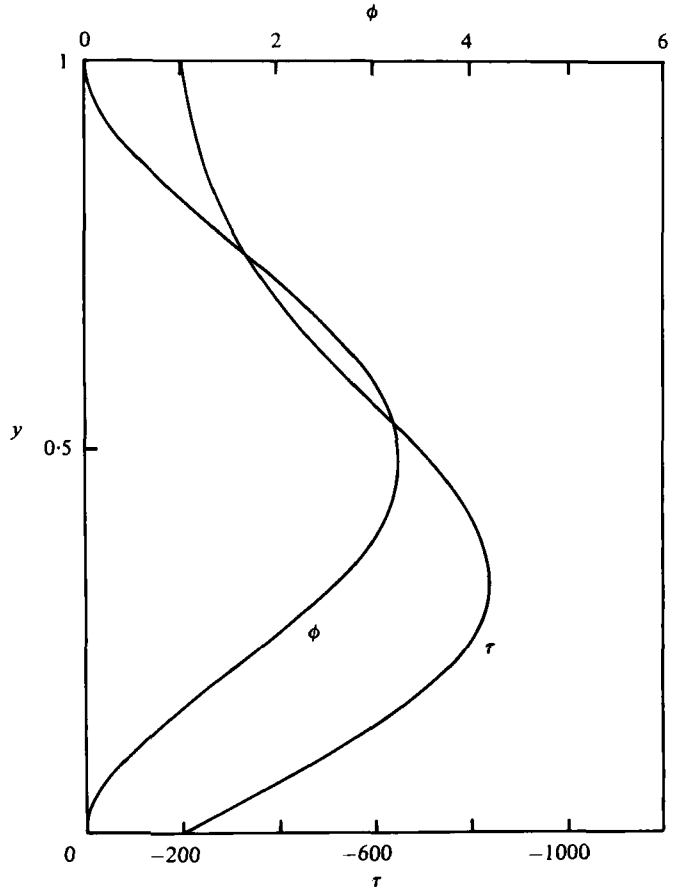

FIGURE 9. Effect of wall temperature variation on the streamfunction and temperature profiles ($B = -200$, $Pr \to \infty$).

The effect of wall temperature variation can be illustrated using the numerical scheme described already in § 3. We assume a wall temperature of the form

$$\theta = x^2 B, \tag{27}$$

where B is a negative number accounting for the fact that in an experimental situation the temperature of the mouth-end of the wall is pulled towards the reservoir temperature. In the numerical scheme, the temperature boundary condition (22) is replaced by

$$\tau = B \quad \text{at} \quad y = 0, 1. \tag{28}$$

In figure 9 we show the streamfunction and temperature profiles obtained in the case $B = -200$ ($Pr \to \infty$). Comparing these results with figures 2 and 4 we find that the extrema of $\phi(y)$ and $\tau(y)$ become less pronounced as B increases in absolute value. The decrease in $\phi_{\max}$ means that less reservoir fluid is drawn into the cavity; the decrease in $|\tau_{\min}|$ implies that the penetration length *increases* as the walls respond thermally to the presence of the reservoir [see equation (25)].

In figure 9, the temperature minimum is $\tau_{\min} = -820$, therefore, parameter

$B = -200$ accounts for a situation in which the wall temperature (at $x_* = L_e$) is located 'a quarter of the way' between the two extreme temperatures (closer to temperature of the closed end). Such a situation occurred, approximately, in our own experiment (figure 7). Consequently, using $\tau_{\min} = -820$ in equation (25), the theoretical estimate for penetration length becomes $L_e \cong 6{\cdot}91$ cm; this length is only 8 % shorter than the experimental value 7·5 cm.

Finally, it is worth noting that the Rayleigh number achieved in the present water experiment, $Ra \cong 10^5$, corresponds to an air convection application where $H = 10$ cm if $\Delta T = 1$ °C, or $H = 4{\cdot}5$ cm if $\Delta T = 10$ °C. Vertical dimensions of this magnitude are commonly encountered in the geometry of irregular building walls, particularly in designs (interior or exterior) using the individual brick or the brick-to-brick gap as the most elementary design feature. Our own experiment (figure 8) indicates that lateral penetration will also be present between adjacent fins on the water side of a heat-exchanger surface.

5. Conclusions and applications

We presented a theoretical and experimental study of penetration by free convection into a lateral cavity communicating with a layer fluid reservoir at a different temperature. The important parameter of the flow is the Rayleigh number Ra based on cavity height H and cavity–reservoir temperature difference. The flow pattern and the predicted penetration length agreed well with experimental observations. We also found that Ra must exceed $1{\cdot}2 \times 10^3$ if free convection is to penetrate laterally to a length greater than the cavity height.

As a first engineering application of the results obtained in this study, we can evaluate the net heat exchange between the cavity walls and the reservoir fluid. Integrating the heat flux over the horizontal walls of the cavity, figure 1, we find

$$\frac{Q}{W} = \int_0^{L_e} \left[-k \left(\frac{\partial T_*}{\partial y_*} \right)_{y=1} + k \left(\frac{\partial T_*}{\partial y_*} \right)_{y=1} \right] dx_*, \tag{29}$$

where Q, W and k are the net heat exchange, cavity width, and fluid thermal conductivity, respectively. Omitting the algebra, equation (29) can be rewritten as

$$Nu = C\, Ra^{\frac{1}{4}}, \tag{30}$$

where the Nusselt number is defined as $Nu = Q/(Wk\Delta T)$. The numerical coefficient C depends on the Prandtl number and is given by

$$C = \frac{\tau'_{y=1} - \tau'_{y=0}}{3(-\tau_{\min})^{\frac{1}{4}}}. \tag{31}$$

Table 1 lists the value of this coefficient, showing that in the Pr range 0·7 to ∞ the Prandtl number has a very weak impact on the Nu–Ra relation (30).

We obtain an estimate of the heat transport enhancement associated with lateral penetration, by comparing the Nusselt number, equation (30), with the corresponding number for a vertical plate of height H blocking the entrance,

$$Nu = 0{\cdot}671\, Ra^{\frac{1}{4}}. \tag{32}$$

This result, reproduced here from Gebhart (1971), corresponds to $Pr \gg 1$. Comparing equations (30), (32) we conclude that the heat transfer rate 'with' lateral cavity exceeds the rate 'without' cavity by the factor $0{\cdot}079\,Ra^{\frac{1}{4}}$. This factor exceeds unity when $Ra > 2{\cdot}6 \times 10^4$, i.e. when the penetration slenderness ratio L_e/H exceeds 4·7. It must be kept in mind that the heat transfer enhancement factor $0{\cdot}079\,Ra^{\frac{1}{4}}$ represents a lower bound, for two reasons. First, the vertical boundary layer thickness for the wall without cavity is greater than assumed in (32), because it is dictated by the wall height which, as in our experiment, is greater than the height of any cavity. Second, the presence of a lateral cavity has the added effect of breaking up the boundary layer lining the vertical wall. The resulting effect is that the heat transfer rate will be increased over that section of vertical wall situated downstream of the lateral opening.

As a final remark, we note that in our presentation we made a special effort to consistently describe the penetration phenomenon as occurring in a warm cavity facing a cold reservoir. The same flow will occur if the cavity is cold and the reservoir is warm. However, to visualize this flow it is necessary to rotate by 180° the pattern illustrated in figure 5.

This research was supported by the National Science Foundation through grant ENG-7820957. The experimental apparatus was constructed by Mr Karl Rupp.

REFERENCES

BAKER, D. J. 1966 A technique for the precise measurement of small fluid velocities. *J. Fluid Mech.* **26**, 573.

BAYLEY, F. J. & MARTIN, B. W. 1971 A review of liquid cooling of high-temperature gas-turbine rotor blades. *Proc. Inst. Mech. Eng.* **185**, 219.

BEJAN, A. 1980 Natural convection in a vertical cylindrical well filled with porous medium. *Int. J. Heat Mass Transfer*, **23**, 726.

CARNAHAN, B., LUTHER, H. A. & WILKES, J. O. 1969 *Applied Numerical Methods*, p. 405. Wiley.

GEBHART, B. 1971 *Heat Transfer*, 2nd edn., p. 336. McGraw-Hill.

HASEGAWA, S., NISHIKAWA, K. & YAMAGATA K. 1963 Heat transfer in an open thermosyphon. *Bull. J.S.M.E.* **6**, 22.

HOOKE, R. & JEEVES, T. A. 1961 Direct search solution of numerical and statistical problems. *J. A.C.M.* **8**, 212.

LIGHTHILL, M. J. 1953 Theoretical considerations on free convection in tubes. *Quart. J. Mech. Appl. Math.* **6**, 398.

MARTIN, B. W. 1955 Free convection in an open thermosyphon, with special reference to turbulent flow. *Proc. Roy. Soc.* A **230**, 502.

MARTIN, B. W. 1959 Free-convection heat transfer in the inclined open thermosyphon. *Proc. Inst. Mech. Eng.* **173**, 761.

MARTIN, B. W. & COHEN, H. 1954 Heat transfer by free convection in an open thermosyphon tube. *B. J. Appl. Phys.* **5**, 91.

PHILLIPS, O. M. 1966 On turbulent convection currents and the circulation of the Red Sea. *Deep-Sea Res.* **13**, 1149.